Multivalent weak interactions enhance selectivity of interparticle binding

M. R. W. Scheepers[a,b], L. J. van IJzendoorn[a,b], and M. W. J. Prins[a,b,c,1]

[a]Department of Applied Physics, Eindhoven University of Technology, 5600 MB Eindhoven, The Netherlands; [b]Institute for Complex Molecular Systems, Eindhoven University of Technology, 5600 MB Eindhoven, The Netherlands; and [c]Department of Biomedical Engineering, Eindhoven University of Technology, 5600 MB Eindhoven, The Netherlands

Edited by Daan Frenkel, University of Cambridge, Cambridge, United Kingdom, and approved July 27, 2020 (received for review March 29, 2020)

Targeted drug delivery critically depends on the binding selectivity of cargo-transporting colloidal particles. Extensive theoretical work has shown that two factors are necessary to achieve high selectivity for a threshold receptor density: multivalency and weak interactions. Here, we study a model system of DNA-coated particles with multivalent and weak interactions that mimics ligand–receptor interactions between particles and cells. Using an optomagnetic cluster experiment, particle aggregation rates are measured as a function of ligand and receptor densities. The measured aggregation rates show that the binding becomes more selective for shorter DNA ligand–receptor pairs, proving that multivalent weak interactions lead to enhanced selectivity in interparticle binding. Simulations confirm the experimental findings and show the role of ligand–receptor dissociation in the selectivity of the weak multivalent binding.

multivalency | selectivity | particles

Multivalent interactions are omnipresent in biology as these enable interactions that are strong, reversible, and highly selective (1–3). Multiple individually weak noncovalent interactions cooperatively form a highly specific multivalent bond between biological entities that can have molecular as well as cellular dimensions (4, 5).

These principles are also exploited in nanomedicine to develop nanoparticles that target specific cell types in order to improve diagnosis and treatment (6–8). The targeting relies on identifying membrane receptor signatures that are unique to the targeted cell. However, in many diseases it is not the receptors but rather the receptor expression levels that are different for diseased cells compared to healthy cells (9, 10). Therefore, the drug delivery particles should exhibit receptor-density specificity, that is, the particles should bind as selectively as possible to cells with a receptor density above a certain threshold density (Fig. 1*A*).

The group of Frenkel in Cambridge has done extensive theoretical work on the topic of receptor-density specificity. They have developed a statistical mechanical model that describes the interaction between ligand-coated guest particles and a receptor-coated host substrate (11). The model yields the fraction of bound guest particles θ in the equilibrium state as a function of the receptor density. The selectivity of the guest–host binding is quantified by a selectivity parameter α, which is smaller than 1 if the binding has a sublinear dependence on receptor density and larger than 1 if the dependence is faster than linear (superselectivity). The works of Frenkel and other groups predict that a high receptor-density specificity can be achieved by using particles that interact in a multivalent fashion with a cell membrane (11–15). Interestingly, the selectivity increases when the equilibrium association constant K_a of an individual ligand–receptor pair decreases (11, 16, 17). In other words, many weak bonds are more selective than a single strong bond.

Several experimental studies have proven parts of Frenkel's theoretical work. Albertazzi et al. (18) showed superselectivity in self assembling of a supramolecular polymer by introducing a multivalent binder. Dubacheva et al. (19) showed superselective binding for a model system of multivalent hyaluronic acid polymers binding to a functionalized surface. In these experiments the equilibrium concept of superselectivity has been proven for the binding of multivalent polymers. However, these papers did not study any kinetic aspects, that is, how multivalent systems change their kinetic binding probability as a function of the number of receptors, and also did not study selectivity properties of biofunctionalized colloidal particles.

Here, we study how interparticle kinetic rates depend on the number of interacting receptors, as a mimic of particle–cell interactions (Fig. 1*B*). Colloidal particles are suspended in solution, where half of the particles are coated with ligands at a surface density σ_L, called the ligand particles (L), and the other half of the particles are coated with receptors at a surface density σ_R, called the receptor particles (R). We use a DNA model system in which ligand DNA and receptor DNA consist of single-stranded overhangs, exposed from 20-bp double-stranded DNA fragments. When two particles ($R = 250$ nm) are in close proximity, multiple ligand–receptor bonds can be formed, depending on the binder densities. By changing the length of the single-stranded overhangs, that is, changing the number of complementary bases, the strength of the individual ligand–receptor bonds can be tuned.

To quantify the binding between the ligand and receptor particles, we measure the interparticle aggregation rate k_{agg} using a previously developed optomagnetic cluster (OMC) experiment (20). The parameter k_{agg} represents the rate at which biochemical interparticle aggregation occurs, for particles that are in a well-defined state of proximity. Briefly, a dispersion of superparamagnetic particles is exposed to an external magnetic field.

Significance

The selectivity of binding of colloidal particles is an important research topic for the field of targeted drug delivery. Extensive theoretical work has shown that high selectivity can be obtained by using multivalent weak interactions. Here we provide comprehensive experimental proof using DNA-coated particles. The ligand–receptor affinity is varied by changing the number of complementary bases, showing that fewer complementary bases yield a higher binding selectivity. The experimental data and corresponding numerical model simulations demonstrate the scaling behavior between molecular density, molecular affinity, and resulting density selectivity of interparticle binding. These results are important for the design of novel systems for targeted nanoparticle drug delivery.

Author contributions: M.R.W.S., L.J.v.IJ., and M.W.J.P. designed research; M.R.W.S. performed research; M.R.W.S. analyzed data; and M.R.W.S., L.J.v.IJ., and M.W.J.P. wrote the paper.

The authors declare no competing interest.

This article is a PNAS Direct Submission.

See online for related content such as Commentaries.

[1]To whom correspondence may be addressed. Email: m.w.j.prins@tue.nl.

This article contains supporting information online at https://www.pnas.org/lookup/suppl/doi:10.1073/pnas.2003968117/-/DCSupplemental.

First published August 28, 2020.

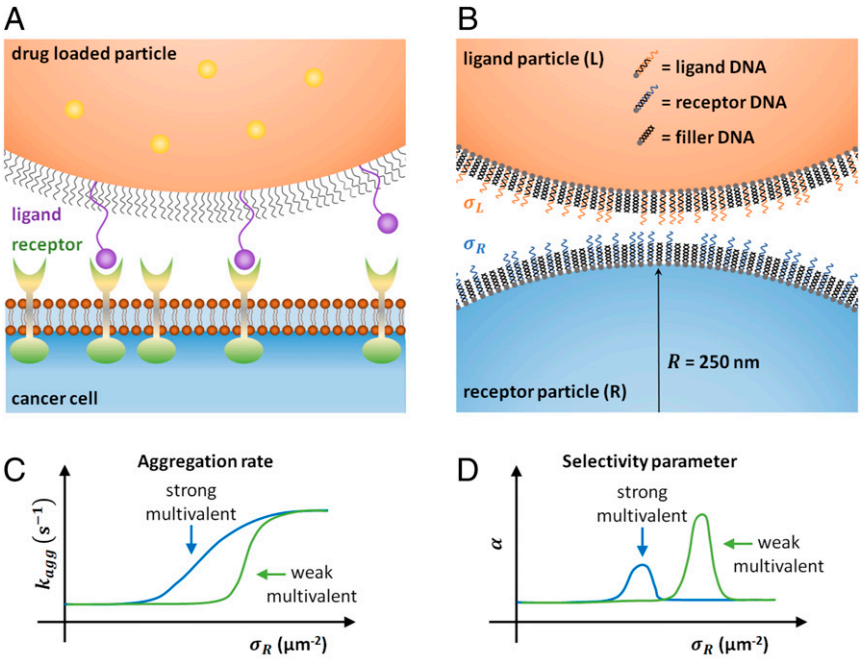

Fig. 1. Particle–particle interaction mimics cell–particle interactions. (*A*) Multivalent binding of a ligand-coated particle to receptors on a cell membrane. (*B*) Ligand particles are coated with short DNA constructs with a single-stranded overhang, called ligand DNA. Receptor particles are coated with short DNA constructs with a complementary single-stranded overhang, called receptor DNA. The overhang complementarity determines the strength of the ligand–receptor interaction. Filler double-stranded DNA strands, without single-stranded overhang, are inserted to maintain a constant surface charge density. (*C*) The aggregation rate is measured as a function of the receptor density, for a constant ligand density. Weaker interactions, with fewer complementary nucleotides in the single-stranded overhang of the receptor strand, cause a higher selectivity of interparticle binding. (*D*) The selectivity parameter α is calculated from the dependence of aggregation rate on receptor density. Weak multivalent interactions yield enhanced selectivity compared to strong multivalent interactions.

The attractive interparticle magnetic force brings particles in a well-defined proximal state where interparticle ligand–receptor bonds can be formed. After a fixed interaction time the external field is turned off. At that point, unbound particle dimers fall apart and dimers bound by at least a single ligand-receptor bond remain. The number of biochemically bound dimers is recorded as a function of time, which allows the quantification of the average interparticle aggregation rate k_{agg}. A complete description of the OMC experiment is given in *SI Appendix*, section S1.

In this paper, we experimentally study how the kinetics of particle–particle binding scales with the density of ligands, density of receptors, and their interaction strengths. The selectivity parameter is quantified for complementary DNA lengths ranging from 15 bp to as few as 5 bp, that is, from strong to very weak interactions. Additionally, a simulation model is presented which elucidates that enhanced selectivity can be obtained by only increasing the dissociation rate of the ligand–receptor pairs. The paper concludes with a discussion about how the obtained results can be interpreted for applications in targeted drug delivery.

Materials and Methods

Materials. Streptavidin-coated superparamagnetic Ademtech Masterbeads were purchased from Ademtech (diameter 528 nm, coefficient of variation 25%). Biotinylated DNA strands were purchased from IDT (for a complete list of the DNA sequences used, see *SI Appendix*, section S2). Phosphate-buffered saline (PBS) tablets, bovine serum albumin (BSA, >98% pure), biotin-Atto655, and Protein LoBind Eppendorf tubes were obtained from Sigma-Aldrich. Borosilicate glass 3.3 cuvettes with inner dimensions of 1.00 ± 0.05 mm × 1.00 ± 0.05 mm and outer dimensions of 1.23 ± 0.05 mm × 1.23 ± 0.05 mm and a length of 20 ± 1 mm were obtained from Hilgenberg GmbH.

Particle Functionalization. Particles were functionalized in a fashion similar to that presented in previous work (21). Briefly, streptavidin-coated Ademtech Masterbeads were functionalized with biotinylated ligand or receptor DNA strands and filler DNA strands by sequential incubation steps. First, 15 μL of the particle stock solution (10 mg/mL) was mixed with 285 μL of ligand DNA or receptor DNA solution in PBS and incubated for 60 min in an incubator shaker (1,200 rpm, room temperature). Subsequently 2 μL of a large excess of filler DNA was added to saturate the remaining streptavidin groups with DNA and incubated for 60 min in an incubator shaker (1,200 rpm, room temperature). The amount of functional ligand DNA or receptor DNA strands on the particle was varied throughout the experiments. After the second incubation step, the particle solution was magnetically washed to remove the unbound DNA strands. The particles were redispersed in a 10 mg/mL BSA in PBS solution to suppress nonspecific aggregation of the particles. The particle solution was then incubated in a sonic bath for 10 min and the solution was sonicated (10 × 0.5 s) to reduce the number of background clusters in the solution.

Supernatant Assay for DNA Docking Strand Coverage Quantification. To quantify the number of DNA strands on the streptavidin-coated Ademtech Masterbeads an indirect fluorescence supernatant assay was performed, similar to that in our previous work (21). First, the biotin capacity of the particles was quantified by binding increasing amounts of biotin-atto655 (b-atto655) on the particles, during 60 min in an incubator shaker (1,200 rpm, room temperature). The lowest b-atto655 concentration at which there is still b-atto655 left over in the supernatant after incubation was quantified using a Thermo Fischer Fluoroskan Ascent FL (λ_{ex} = 646 nm, λ_{em} = 679 nm, spectral width 5 nm) (*SI Appendix*, Fig. S3*A*). The b-atto655 capacity per particle was equal to $N_{b\text{-}atto655} = (7.3 \pm 0.6) \cdot 10^4$.

Next, increasing amounts of ligand or receptor biotinylated DNA were added to the particles and incubated during 60 min in an incubator shaker (1,200 rpm, room temperature). After this incubation step, the particle solution was magnetically washed to remove unbound DNA strands. Subsequently, b-atto655 was added in a concentration that was slightly above the b-atto655 capacity of the particles followed by an incubation step of 60 min in an incubator shaker (1,200 rpm, room temperature). Particles that were not fully coated with DNA strands bind some of the b-atto655 in the solution, while the fully coated particles do not bind any b-atto655 anymore. After the

incubation the particle solutions were magnetically washed and the fluorescence of the supernatant was measured. The amount of b-atto655 in the supernatant for a certain DNA concentration, $I_{s.n.}([DNA])$, is related to the number of DNA on the particle, N_{DNA}, according to Eq. **1**:

$$N_{DNA} = \frac{I_0 - I_{s.n.}([DNA])}{I_0 - I_{s.n.}([DNA]=0)} \cdot N_{b-atto655}. \quad [1]$$

Here I_0 is the fluorescence intensity of the b-atto655 solution that is added in the second incubation step, and $I_{s.n.}([DNA]=0)$ is the fluorescence intensity of the supernatant when adding nonfunctionalized streptavidin Ademtech Masterbeads. For more details of the supernatant assay see *SI Appendix*, section S3.

Aggregation Rate as a Function of Receptor and Ligand Density

We investigate how the binding between colloidal particles depends on the ligand and receptor densities, using the DNA model system of Fig. 1*B*. Streptavidin-coated Ademtech Masterbeads were functionalized with three different biotinylated DNA constructs: ligand DNA, receptor DNA, and filler DNA. Ligand DNA strands consist of a 20-bp double-stranded DNA spacer with a 15-nt single-stranded overhang. Receptor DNA strands also consist of a 20-bp double-stranded spacer, but they have a single-stranded overhang that varies from 5 up to 15 nt. The filler DNA consists only of the 20-bp double-stranded spacer and is used to saturate the particle with DNA, such that the surface charge of the particle remains constant throughout the experiments.

The streptavidin-coated particles were sequentially incubated for 1 h, first with a certain concentration of either ligand or receptor DNA to obtain a certain ligand or receptor coverage and subsequently with an excess of filler DNA to saturate the particle surface (a complete description of the functionalization process is given in *Materials and Methods*). To quantify the number of functional DNA strands that bind to the particles during the 1-h incubation, a supernatant assay was performed (the supernatant assay is described in detail in *SI Appendix*, section S3). *SI Appendix*, Fig. S3*B* shows the dependence of the bound DNA surface density as a function of the incubated DNA surface density, calculated by dividing DNA concentration by particle concentration. The measured curve follows a linear relation until a plateau is reached. The DNA surface density of this plateau represents the DNA capacity of the particle: $\sigma_{DNA,max} = (2.2 \pm 0.5) \cdot 10^4$ μm^{-2}. The obtained relation between incubated DNA coverage and bound DNA coverage is used in the remainder of this paper, such that the ligand density σ_L or receptor density σ_R always represent bound surface densities.

To quantify the binding between ligand particles and receptor particles, they were mixed in a 1:1 ratio and the aggregation rate was measured using the OMC experiment (20). Fig. 2*A* shows the measured aggregation rate as a function of the receptor density for the 15 complementary base-pair system. The data point at zero receptor density quantifies the nonspecific interaction between the DNA coated particles: $k_{agg,ns} = (5 \pm 2) \cdot 10^{-3}$ s^{-1}. At low receptor densities ($\sigma_R \approx 10^1$ μm^{-2}) the aggregation is dominated by nonspecific interactions between the particles. For ligand densities $\sigma_L > 10^3$ μm^{-2} and receptor densities $\sigma_R \approx 10^2$ μm^{-2}, the measured aggregation rate increases significantly above the nonspecific aggregation rate, and increases nearly linearly with increasing receptor density.

For receptor densities $\sigma_R > 10^3$ μm^{-2}, a plateau is reached at an aggregation rate slightly above $k_{agg} = 0.05$ s^{-1}. This is the highest aggregation rate observed for this system in the OMC experiment. Half of the magnetic dimers that are formed during the actuation time consist of a ligand particle and a receptor particle, allowing for specific DNA hybridization. The other half of the magnetic dimers consist of either two ligand particles or two receptor particles, not allowing for specific binding. *SI Appendix*, Fig. S4 shows that the nonspecific aggregation rate is low and does not depend on receptor density or on the length of the single-stranded overhang.

Fig. 2 *B* and *C* show similar curves for the DNA system with 12- and 9-bp complementarity, respectively. The measured curves, for all ligand densities, resemble the ones of the 15-bp system. This can be understood from the similar association rates and slow dissociation with respect to the experimental time. In the OMC experiment, dimers of particles are magnetically formed and the particles are kept in close proximity for an applied interaction time. It is known from literature that the association rate k_{on} of short DNA strands in solution only very weakly depends on the number of complementary bases (22–24). Therefore, in the experiment roughly the same number of ligand–receptor bonds are expected to be formed for the 15-, 12-, and 9-bp systems. Subsequently, the field is turned off during a waiting time of $t_{wait} = 40$ s, allowing the particles to redisperse in the solution. After the waiting phase the number of bound particle dimers is measured and the aggregation rate is calculated. Dimer dissociation during the waiting phase leads to a lower aggregation rate. However, in all cases (15-, 12-, or 9-bp complementarity) the single-molecular dissociation time (25–27) is significantly higher than the waiting time of 40 s, so dimer dissociation is not expected in the OMC experiment. Thus, we attribute the similarity of the curves in Fig. 2 *B* and *C* for the 15-, 12-, and 9-bp DNA to their similar association rates and slow dissociation with respect to the experimental time.

The results are very different for the 8-, 7-, and 5-bp systems. Fig. 2 *D*–*F* show the aggregation rate as a function of the receptor surface density. The curves have a steep dependence on receptor density, which implies a higher selectivity parameter than for the high-affinity interactions (15/12/9 bp). The receptor-density onset, that is, the threshold where aggregation occurs, increases with decreasing ligand density and with decreasing number of complementary bases. This is in qualitative agreement with the theoretical predictions of Wang and Dormidontova (17). Note that particle aggregation is observed even for the 5-bp interaction, for which the single-molecular dissociation time (27) is about 1 s, which is much shorter than the waiting time of 40 s in the OMC experiment. Still, particle aggregation is clearly observed at high receptor densities, which must therefore be due to the presence of multivalent bonds between the particles in a dimer.

Enhanced Selectivity for Weak Multivalent Interactions

To quantify and compare the selectivity of the ligand–receptor binding for different DNA lengths, the aggregation rate curves for ligand density $\sigma_L = (2.2 \pm 0.5) \cdot 10^4$ μm^{-2} for all DNA lengths are fitted and plotted in one graph (Fig. 3*A*). The measured curves are fitted using a sigmoid curve. Details about the fitting can be found in *SI Appendix*, section S5.

In Fig. 3*A* the gray dotted line indicates the receptor density above which it is possible to form multiple bonds. The estimation is based on the radius of the particle, the length of a ligand–receptor bond, and the interparticle distance (for the complete calculation see *SI Appendix*, section S6). At receptor densities left from the dotted line, there is on average at most one receptor present in the interaction area, which is the area on the receptor particle that is at a distance from the ligand particle of at most a bond length ($L_{bond} \sim 20$ nm). For the DNA lengths for which a single bond is stable on time scales of the waiting time—15, 12, and 9 bp—there is significant specific aggregation at receptor densities in the monovalent regime. For the weaker interaction—8, 7, and 5 bp—higher receptor densities are necessary to allow for particle aggregation by multivalent binding.

The selectivity parameter α is defined by Martinez-Veracoechea and Frenkel (11) as the relative change in the number of bound

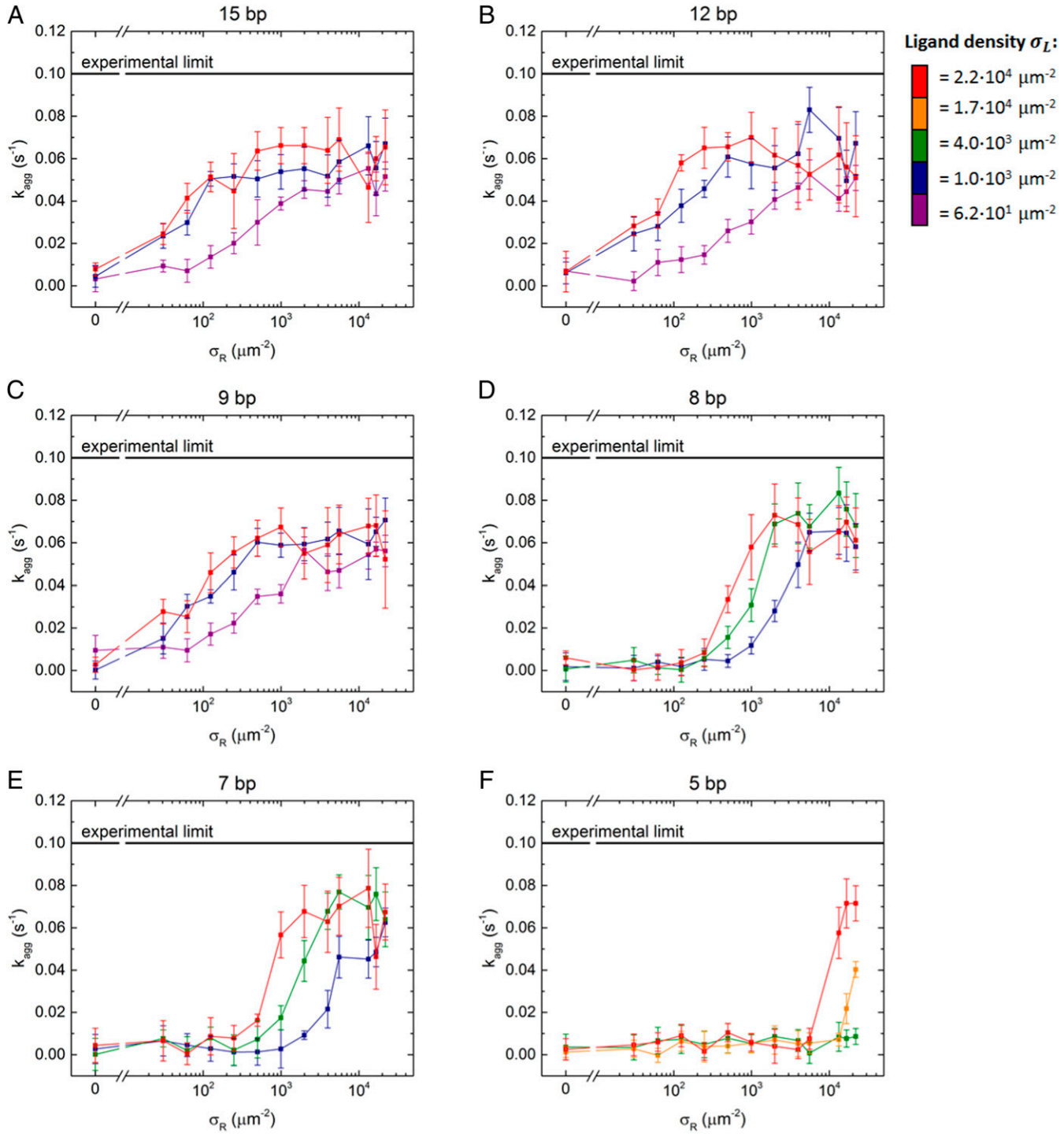

Fig. 2. Aggregation rate as a function of receptor density (σ_R), ligand density (σ_L) and ligand–receptor affinity (bp): (*A*) 15-bp, (*B*) 12-bp, (*C*) 9-bp, (*D*) 8-bp, (*E*) 7-bp, and (*F*) 5-bp complementary between ligand and receptor.

particles N_{bound} formed in equilibrium, as a function of the number of receptors on a cell n_R: $\alpha = \frac{d \ln N_{bound}}{d \ln n_R}$. In the OMC experiment, we measured the rate of interparticle binding k_{agg}, which represents the number of bound dimers divided by the mean interaction time, as a function of the receptor density σ_R, which is the number of receptors divided by the particle area. Since α describes a relative change in the number of bound particles with the number of receptors, we can multiply N_{bound} and n_R by any nonzero constant, without changing α. Thus, we can replace N_{bound} and n_R by $k_{agg}\langle t_{int}\rangle$ and $\sigma_R A_{particle}$, respectively, to achieve the following expression:

$$\alpha = \frac{d \ln N_{bound}}{d \ln n_R} = \frac{d \ln \left(k_{agg} \cdot \langle t_{int} \rangle\right)}{d \ln \left(\sigma_R \cdot A_{particle}\right)}. \quad [2]$$

With this equation and the fitted curves of Fig. 3*A*, the selectivity parameter is calculated as a function of the receptor density (Fig. 3*B*). The shaded bands around the solid curves are obtained

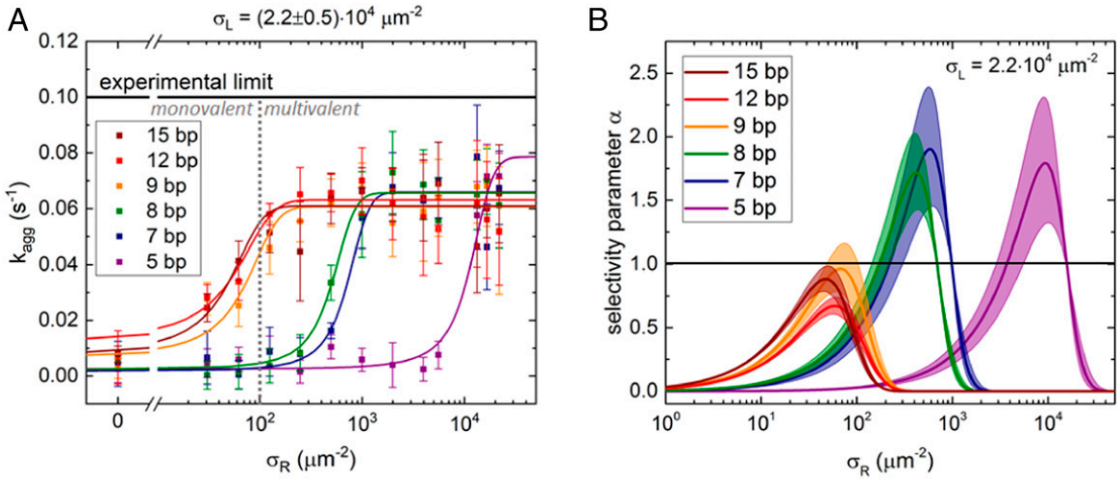

Fig. 3. Enhanced selectivity for weak multivalent interactions. (*A*) Measured aggregation rates as a function of receptor density for a constant ligand density of $\sigma_L = (2.2 \pm 0.5)\ 10^4\ \mu m^{-2}$ for all interaction strengths. Left of the dotted line, on average less than one receptor is present in the interaction area; to the right of the dotted line, on average more than one receptor is present. The 15-, 12-, and 9-bp data are fitted with an exponential function and the 8-, 7-, and 5-bp data are fitted with a sigmoidal function. Details about the fitting can be found in *SI Appendix*, section S4. (*B*) Calculated selectivity parameter using Eq. **2**, with the fit parameters obtained from A. The weak ligand–receptor interactions (5/7/8 bp) yield an enhanced selectivity compared to the strong ligand–receptor interactions (9/12/15 bp).

from the fit errors and represent the uncertainty interval in the selectivity parameter. The measured aggregation curves have an S-like shape. At low aggregation rates (in the range of $k_{agg} < 0.01\ s^{-1}$), the aggregation process is dominated by nonspecific interactions between the particles; here, the rate does not depend on the receptor density and the experimentally determined selectivity equals zero. For increasing receptor densities, the selectivity parameter α reaches 1 at the curve inflection and returns to zero when the aggregation rate saturates. The measured selectivity for the 15-, 12-, and 9-bp interactions ranges between zero and unity, meaning that the measured aggregation rate increases at most linearly with receptor density. In contrast, the selectivities for the 8-, 7-, and 5-bp interactions reach almost the value 2, meaning that the measured aggregation rate increases up to quadratically with receptor density. This proves that the multivalent weak interactions lead to enhanced selectivity in interparticle binding.

Aggregation Rate Simulations

To further investigate the experimentally measured binding selectivities, a kinetic Monte Carlo simulation has been developed that mimics the ligand–receptor-induced particle binding. The aim of the simulation is to understand the origin of the enhanced selectivity for the weak multivalent interactions and assess the relevance of the results for conditions beyond the experimental scope.

In the simulation, particles have either a ligand density σ_L or a receptor density σ_R. During the magnetic actuation time t_{act}, particle dimers are formed at a constant rate k_{dim}^{mag}. Here monomer depletion and the formation of larger clusters are neglected (see SI Appendix, section S5 of ref. 20). Within the magnetic dimers, it is not trivial to model the surface-to-surface distance of the particles, because the interparticle distance results from the sum of several interparticle forces with different signs and length ranges, for example the Hamaker force, electrostatic forces, the magnetic force, entropic forces such as the hydrophobic effect and steric repulsion, and the depletion force; in addition, surface roughness can be important (28). To enable a calculation starting from the basic force equations, one would need to know the underlying particle parameters with high precision, which is not the case for the particles used in this study. Therefore an approach is needed with a limited number of parameters, in order to allow a comparison with the experimental results.

What we know in the experiments is that the DNA density on each particle is equal, because ligand and receptor DNA were complemented with filler DNA. This means that the charge and sterically induced interparticle repulsion can be approximated to be constant in the experiments. Also, the magnetic force can be assumed to be constant, because the magnetic actuation field was constant. The formation of single-molecular bonds can add attractive as well as repulsive contributions to the interparticle potential, for example due to the finite length of the bond (20 nm) and the mechanical rigidity of the hybridized construct. However, every hybridized construct has four hinge points, namely two hinges at the points of attachment to the particles and two hinges at the starting bases of the single-stranded overhangs, causing the interparticle bonds to be quite flexible. Furthermore, the number of bonds is much smaller than the total number of DNA molecules in the interparticle interaction area (estimated to be about 1,000 including DNA filler molecules), limiting the influence of the constructs on the overall interparticle potential. Thus, the interparticle distance is not a priori known, but we assume that the particles have the minimum of their interaction potential at an effective interparticle distance Δx that is constant during the actuation time. The interparticle distance is a parameter that defines the geometrical overlap between ligand and receptor molecules, so it is interesting to model how the particle aggregation rate would scale with different values of the interparticle distance.

We model the particles as spheres with radius R of which either ligand or receptor DNA molecules protrude from the surface. The probability that a dimer consists of a receptor particle and a ligand particle is 50%. Each dimer has an individual interaction time t_{int}, equal to the time between the moment that the dimer is formed and the end of the actuation time. During this interaction time the particles in a dimer can form one or more ligand–receptor bonds, depending on the number of geometrically overlapping ligand and receptor molecules and their effective association and dissociation rates.

The intrinsic binding rate k_{LR} [$\mu m^2\ s^{-1}$] is defined as the rate at which ligand–receptor bonds are formed between a particle with unit ligand density σ_L and a particle with unit receptor density σ_R. Because the particle surfaces are curved and the ligand–receptor interaction depends on the distance, k_{LR} represents the average

binding rate over all possible ligand–receptor distances. The maximum distance where a bond can be formed is the length of the ligand–receptor bond. The ligand–receptor bond density σ_{LR} can be calculated numerically according to Eq. **3**:

$$\frac{d\sigma_{LR}}{dt} = k_{LR}\sigma_L\sigma_R - k_{off}\sigma_{LR}. \quad [3]$$

Here k_{off} [s^{-1}] is the rate at which ligand–receptor bonds dissociate. To calculate the total number of interparticle bonds that are formed during the interaction time, first the bond density is calculated numerically and subsequently the total number of bonds is determined using Eq. **4**:

$$N_{LR} = \sigma_{LR}A_{int}. \quad [4]$$

Here A_{int} is the interaction area on the particles, which is defined as the area on the particles where the distance between the two particles is smaller than the length of the hybridized DNA construct $L_{bond} \approx 20$ nm, so that DNA–DNA bonds can be formed. The size of the interaction area depends on the interparticle distance Δx, because a larger interparticle distance reduces the area where ligand and receptor molecules are overlapping; more details can be found in *SI Appendix*, Fig. S6.

When at least one ligand–receptor bond has been formed during the interaction time, the dimer is called aggregated. Subsequently, during the waiting time t_{wait}, already formed ligand–receptor bonds may dissociate, but simultaneously new bonds can be formed since the particles are still held in close proximity by the already formed bonds. However, when all ligand–receptor bonds are dissociated at some point in time, the dimer is no longer aggregated and cannot be formed again as both criteria for particle confinement (by magnetic attraction or by molecular bonds) disappeared. After the waiting time, only the dimers with strong interparticle bonds remain, that is, dimers with effective dissociation times exceeding the waiting time. The selectivity parameter is therefore representative for these strong bonds. The final number of ligand–receptor bonds inside a dimer is calculated using Eqs. **3** and **4**. Ultimately, a certain fraction of the dimers is aggregated by one or more ligand–receptor bonds. Also, nonspecific interactions are taken into account, by including a nonspecific interaction rate k_{ns} [s^{-1}]. From the total fraction of aggregated dimers, the aggregation rate k_{agg} is calculated according to *SI Appendix*, Eq. **S1**. A complete parameter scan of the simulation is given in *SI Appendix*, section S7. The simulated curves reproduce an S-like shape as seen in the measurements; the aggregation rates increase and the curves shift toward lower receptor concentration in case of a reduction of interparticle distance, increase of intrinsic binding rate, increase of ligand density, and decrease of dissociation rate.

Fig. 4 relates the simulation results to the experimentally measured aggregation rates. The experimental results for the high-affinity interactions (15/12/9 bp) are very similar and therefore these data are averaged and represented by the orange data points in Fig. 4*A*. As mentioned above, molecular dissociation can be neglected for these high affinities, so the dissociation rate can be set to zero and the unknown simulation parameters are Δx and k_{LR}. The other simulation parameters are kept constant (*SI Appendix*, Table S8). Fig. 4*B* and *SI Appendix*, Fig. S8 show that there are multiple combinations of Δx and k_{LR} for which the simulated aggregation rate matches with the measured aggregation rate. Small interparticle distances ($\Delta x \leq 8$ nm) and high ligand–receptor binding rates ($k_{LR} \geq 10^{-5}$ $\mu m^2 \cdot s^{-1}$) are necessary to match the simulation with the experiment. Reducing the interparticle distance below 8 nm (for high k_{LR}) or increasing the ligand–receptor binding rate above 10^{-5} $\mu m^2 \cdot s^{-1}$ (for low Δx) does not change the simulated curve. In these parameter ranges, one ligand and one receptor in the interaction area are enough to form a bond in the given actuation time, so the binding rate is determined solely by the density of molecules. For the same reason, the shape of the orange curve in Fig. 4*A* is determined purely by the probability to have at least a single receptor molecule present in the interparticle interaction area.

Subsequently, the experimental data for the 8-, 7-, and 5-bp DNA interaction is reproduced using the simulation. For each matching combination of Δx and k_{LR} simulations are performed with a varying nonzero dissociation rate. Fig. 4*A* shows the simulated aggregation rate curves for $\Delta x = 4$ nm and $k_{LR} = 10^{-4}$ $\mu m^2 \cdot s^{-1}$ (red dot in Fig. 4*B*), accompanied by the experimental data. The simulation can reproduce the measured data for each DNA length. This indicates that the enhanced binding selectivity for weak affinities can be obtained by modifying only the dissociation rate of the ligand–receptor interaction.

Table 1 gives an overview of the simulated dissociation rates that lead to a match between simulation and experiment, for all

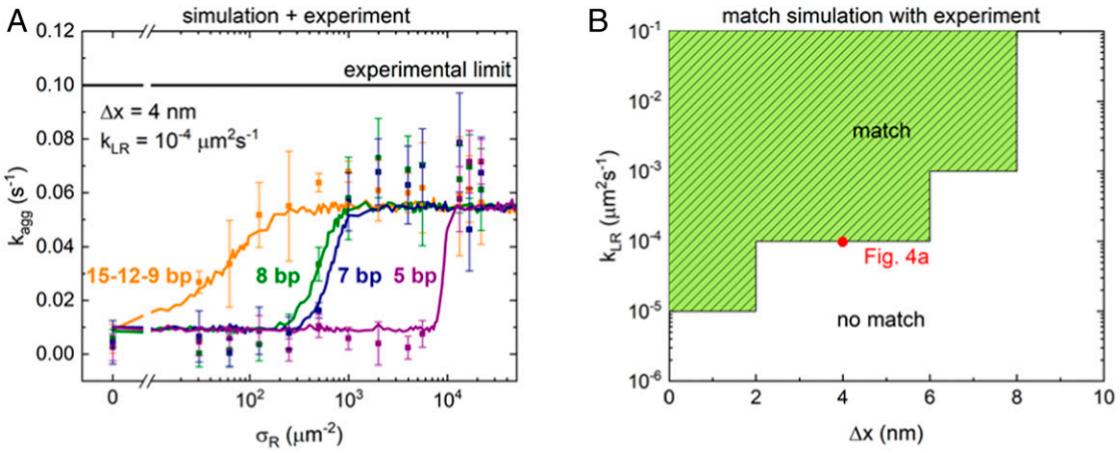

Fig. 4. Simulation results compared to experimental data. (*A*) Experimental data points accompanied by simulated aggregation rate curves for an interparticle distance $\Delta x = 4$ nm and a ligand–receptor binding rate $k_{LR} = 10^{-4}$ $\mu m^2 s^{-1}$. The experimental data of the 15-, 12-, and 9-bp DNA is averaged as these data are very similar. Simulated aggregation rate curves for the other combinations of Δx and k_{LR} are shown in *SI Appendix*, Fig. S8. (*B*) Heat map showing the possible combinations of Δx and k_{LR} for which the simulation reproduces the experimental data. Small interparticle distance and high ligand receptor binding rates lead to a match between simulation and experiment. The red dot shows the specific combination of Δx and k_{LR} for the simulation curves in A.

Table 1. Overview of simulation results

		k_{off} (s^{-1})			$\tilde{K}_a = k_{LR}/k_{off}$ (μm^2)			selectivity α			
Δx (nm)	k_{LR} ($\mu m^2 s^{-1}$)	8bp	7bp	5bp	8bp	7bp	5bp	9 – 15bp	8bp	7bp	5bp
2	10^{-5}	$3.0 \cdot 10^0$	$4.0 \cdot 10^0$	$6.0 \cdot 10^0$	$3.3 \cdot 10^{-6}$	$2.5 \cdot 10^{-6}$	$1.7 \cdot 10^{-7}$	0.5	1.6	1.9	7.2
	10^{-4}	$3.0 \cdot 10^1$	$4.0 \cdot 10^1$	$6.0 \cdot 10^1$							
	10^{-3}	$3.0 \cdot 10^2$	$4.0 \cdot 10^2$	$6.0 \cdot 10^2$							
4	10^{-4}	$2.5 \cdot 10^1$	$3.5 \cdot 10^1$	$4.0 \cdot 10^1$	$4.0 \cdot 10^{-6}$	$2.9 \cdot 10^{-6}$	$2.5 \cdot 10^{-7}$	0.5	1.5	1.9	6.1
	10^{-3}	$2.5 \cdot 10^2$	$3.5 \cdot 10^2$	$4.0 \cdot 10^2$							
6	10^{-4}	$2.0 \cdot 10^1$	$3.0 \cdot 10^1$	$3.5 \cdot 10^1$	$5.0 \cdot 10^{-6}$	$3.3 \cdot 10^{-6}$	$2.9 \cdot 10^{-7}$	0.5	1.4	1.7	5.6
	10^{-3}	$2.0 \cdot 10^2$	$3.0 \cdot 10^2$	z3.5 $\cdot 10^2$							
8	10^{-3}	$1.7 \cdot 10^2$	$2.7 \cdot 10^2$	$3.0 \cdot 10^2$	$5.9 \cdot 10^{-6}$	$3.7 \cdot 10^{-6}$	$3.3 \cdot 10^{-7}$	0.5	1.3	1.7	6.1

Simulations were performed for each consistent combination of the interparticle distance Δx and ligand–receptor binding rate k_{LR}. The dissociation rate k_{off} for which the simulation reproduces the experimental data of the **8**-, **7**-, and **5**-bp DNA was determined for each combination of Δx and k_{LR}. The affinity constant K_a, the ratio of ligand–receptor binding rate k_{LR} and dissociation rate k_{off}, is independent of the used k_{LR} and depends only slightly on the interparticle distance Δx. The selectivity parameter of the simulated aggregation rate curves were extracted by fitting the curves of *SI Appendix*, Fig. S8.

matching combinations of Δx and k_{LR}. The balance between Δx and k_{LR} determines the association process of the particles. Increasing the interparticle distance Δx leads to fewer interacting ligands and receptors but can be compensated by a higher ligand–receptor binding rate k_{LR}. The dissociation of particle dimers is a balance between on the one hand the amount of ligands and receptors and their binding rate (determined by Δx and k_{LR}) and on the other hand the dissociation rate of the individual ligand–receptor bonds k_{off}. For a certain Δx multiple k_{LR} values are possible that range over orders of magnitude. It turns out that for a 10-times-higher binding rate, the corresponding dissociation rate that follows from the simulation is also 10 times higher.

The effective equilibrium affinity constant $\tilde{K}_a$ (units of square micrometers) can be calculated according to Eq. **5** for each simulation in Table 1:

$$\tilde{K}_a = \frac{k_{LR}}{k_{off}}. \qquad [5]$$

The calculated effective affinity constant $\tilde{K}_a$ describes the balance between association and dissociation of the interparticle bonds. The data in Table 1 show that $\tilde{K}_a$ hardly depends on the fit parameters k_{LR} and Δx. The underlying reason is that the affinity constant relates to the position of the slope of the S-curve, that is, the x-axis value of the inflection point of the curve. The scaling of the affinity constants is as expected: For shorter DNA lengths the obtained affinity constant decreases, corresponding to a shift of the aggregation curve toward higher receptor densities.

The obtained effective affinity constants $\tilde{K}_a$ are defined in terms of surfaces but can be converted to volume affinity constants K_a and then compared with volume affinity constants calculated for DNA sequences in solution (for details see *SI Appendix*, section S9).

SI Appendix, Table S9 shows that the K_a derived from $\tilde{K}_a$ is weaker than the volume affinity constant calculated from the DNA sequence. For example, for the 7-bp DNA the experimentally derived $K_a = 4 \cdot 10^1$ M^{-1} is significantly lower than the calculated affinity constant $K_a = 8 \cdot 10^7$ M^{-1}. Several factors can be identified that might be responsible for this lower affinity. The most probable reason is that the reduced molecular mobility and accessibility on a surface gives a much smaller free energy difference for hybridization on a surface than for hybridization in solution, as has theoretically been treated by Varilly et al. (29). Furthermore, hybridization on the surface may be hindered by the negative electrostatic charge caused by the high density of DNA molecules on the particles.

The selectivity parameter can be extracted from the simulation results (Table 1). The selectivity values increase with decreasing DNA length. This is in agreement with the experimental observation that the selectivity increases with decreasing ligand–receptor affinity. The selectivity parameters resemble the measured values shown in Fig. 3*B* for all DNA lengths except for the 5-bp DNA. However, the discrepancy for the 5-bp DNA is likely due to the limited data points in the rising edge of the experimental curve.

In this paper we measured the aggregation rate of DNA-coated particles to mimic cell–particle binding. In the OMC experiment, the particles are held quasi-continuously in close proximity ($\langle t_{int} \rangle = 10$ s). The interaction time is long enough to form multiple weak ligand–receptor bonds, which together form a stable bond between the particles. However, when identical particles were freely dispersed in a solution, the proximity time would be much shorter. If the proximity time is shorter than the typical time to form a single ligand–receptor bond, particle aggregation is very unlikely to occur.

We calculate the interaction time for particles free in solution using the diffusivity of the particles. For particles with radius $R = 0.25$ μm in an aqueous solution with viscosity $\eta = 1$ mPa·s, the typical time in which a particle diffuses a distance equal to the ligand–receptor bond length $L_{bond} = 0.02$ μm is calculated by Eq. **6**:

$$\tau_{prox} = \frac{\pi \eta R L_{bond}^2}{k_B T}. \qquad [6]$$

This gives a proximity time of $\tau_{prox} = 0.1$ ms. In the OMC experiment such short actuation times cannot be applied, but we can calculate the number of ligand–receptor bonds that would be formed during this proximity time, using Eqs. **3** and **4**. For the highest ligand and receptor densities that were experimentally assessed in this study, $\sigma_L = \sigma_R = 2.2 \cdot 10^4$ μm^{-2}, and a typical ligand–receptor association rate in solution of 10^5 M^{-1} s^{-1} that corresponds to $k_{LR} = 10^{-2}$ $\mu m^2 \cdot s^{-1}$, in combination with a dissociation rate of $k_{off} = 10^3$ s^{-1}, we obtain an average number of five bonds per dimer. This implies that during a single particle-to-particle encounter a stable multivalent bond would in principle be formed between the particles, even for the low-affinity binders. These calculations suggest that superselective particle binding might also be measurable for particles free in solution, without applying any magnetic forces. However, assays without magnetic force will require much longer incubation times than assays with magnetic force (20).

Conclusion

In this paper, the selectivity was studied of the multivalent binding between DNA-coated colloidal particles, quantified by the rate of aggregation observed in an OMC experiment. The aggregation rate was measured for a broad range of receptor and ligand densities, showing how increasing densities lead to increasing aggregation rates. A selectivity parameter is defined as the relative increase in the number of particle dimers as a function of the receptor density on the particles, where a selective binding process is characterized by a selectivity parameter exceeding 1. For DNA receptors with different numbers of complementary bases, from 15 to 5 bp, the following selectivity parameters were obtained: $\alpha_{15bp} = 0.9 \pm 01$, $\alpha_{12bp} = 0.7 \pm 0.1$, $\alpha_{9bp} = 1.0 \pm 0.2$, $\alpha_{8bp} = 1.7 \pm 0.3$, $\alpha_{7bp} = 1.9 \pm 0.5$, and $\alpha_{5bp} = 1.8 \pm 0.5$. These results prove that weaker ligand–receptor affinities lead to higher selectivity parameters. This experimental dataset demonstrates the scaling behavior between molecular affinity and density selectivity of specific binding between colloidal particles.

A kinetic Monte Carlo simulation was developed based on the geometrical overlap between ligand and receptor molecules on the particles, with the particle-to-particle distance and the intrinsic binding and unbinding rates as parameters. The simulated curves reproduce the shapes of the experimentally measured curves and effective areal equilibrium binding affinity constants could be extracted for the different hybridization lengths. The simulation indicates that the enhanced selectivity for a weaker ligand–receptor affinity can be explained by only an increase in the dissociation rate of ligand and receptor. The simulation results show the importance of the proximity time of the particles for the possibility to form multivalent bonds. The results from the described experiments and model prove the existence of superselectivity in the kinetic binding rate of multivalent particle–particle interactions. This work goes beyond equilibrium studies, by gaining insight in kinetic properties, which are relevant for the design of drug delivery systems in terms of particle size, ligand density and ligand–receptor affinity.

Data Availability. All study data are included in the paper and *SI Appendix*.

ACKNOWLEDGMENTS. The authors thank the Peri-Operative IMPULS program for their financial support.

1. A. Gao *et al.*, Evolution of weak cooperative interactions for biological specificity. *Proc. Natl. Acad. Sci. U.S.A.* **115**, E11053–E11060 (2018).
2. C. Fasting *et al.*, Multivalency as a chemical organization and action principle. *Angw. Chem. Int. Ed.* **51**, 10472–10498 (2012).
3. M. Mammen, S. Choi, G. M. Whitesides, Polyvalent interactions in biological systems: Implications for design and use of multivalent ligands and inhibitors. *Angw. Chem. Int. Ed.Engl.* **37**, 2754–2794 (1998).
4. F. Karimi, A. J. O'Connor, G. G. Qiao, D. E. Heath, Integrin clustering matters: A review of biomaterials functionalized with multivalent integrin-binding ligands to improve cell adhesion, migration, differentiation, angiogenesis, and biomedical device integration. *Adv. Healtc. Mater.* **7**, e1701324 (2018).
5. S. Bhatia, L. C. Camacho, R. Haag, Pathogen inhibition by multivalent ligand architectures. *J. Am. Chem. Soc.* **138**, 8654–8666 (2016).
6. P. Y. Liyanage *et al.*, Nanoparticle-mediated targeted drug delivery for breast cancer treatment. *Biochim. Biophys. Acta Rev. Cancer* **1871**, 419–433 (2019).
7. Z. Wang *et al.*, Mechanisms of drug release in pH-sensitive micelles for tumour targeted drug delivery system: A review. *Int. J. Pharm.* **535**, 253–260 (2018).
8. F. He *et al.*, Aptamer-based targeted drug delivery systems: Current potential and challenges. *Curr. Med. Chem.* **27**, 2189–2219 (2018).
9. M. J. Linja *et al.*, Amplification and overexpression of androgen receptor gene in hormone-refractory prostate cancer. *Cancer Res.* **61**, 3550–3555 (2001).
10. M. F. Di Renzo *et al.*, Overexpression of the Met/HGF receptor in ovarian cancer. *Int. J. Cancer* **58**, 658–662 (1994).
11. F. J. Martinez-Veracoechea, D. Frenkel, Designing super selectivity in multivalent nano-particle binding. *Proc. Natl. Acad. Sci. U.S.A.* **108**, 10963–10968 (2011).
12. C. B. Carlson, P. Mowery, R. M. Owen, E. C. Dykhuizen, L. L. Kiessling, Selective tumor cell targeting using low-affinity, multivalent interactions. *ACS Chem. Biol.* **2**, 119–127 (2007).
13. A. Joshi, D. Vance, P. Rai, A. Thiyagarajan, R. S. Kane, The design of polyvalent therapeutics. *Chemistry* **14**, 7738–7747 (2008).
14. B. E. Collins, J. C. Paulson, Cell surface biology mediated by low affinity multivalent protein-glycan interactions. *Curr. Opin. Chem. Biol.* **8**, 617–625 (2004).
15. N. Morel *et al.*, Selective and efficient immunoprecipitation of the disease-associated form of the prion protein can be mediated by nonspecific interactions between monoclonal antibodies and scrapie-associated fibrils. *J. Biol. Chem.* **279**, 30143–30149 (2004).
16. T. Curk, J. Dobnikar, D. Frenkel, Optimal multivalent targeting of membranes with many distinct receptors. *Proc. Natl. Acad. Sci. U.S.A.* **114**, 7210–7215 (2017).
17. S. Wang, E. E. Dormidontova, Selectivity of ligand-receptor interactions between nanoparticle and cell surfaces. *Phys. Rev. Lett.* **109**, 238102 (2012).
18. L. Albertazzi *et al.*, Spatiotemporal control and superselectivity in supramolecular polymers using multivalency. *Proc. Natl. Acad. Sci. U.S.A.* **110**, 12203–12208 (2013).
19. G. V. Dubacheva, T. Curk, R. Auzély-Velty, D. Frenkel, R. P. Richter, Designing multivalent probes for tunable superselective targeting. *Proc. Natl. Acad. Sci. U.S.A.* **112**, 5579–5584 (2015).
20. M. R. W. Scheepers, A. R. Romijn, L. J. van IJzendoorn, M. W. J. Prins, Rate of dimer formation in stable colloidal solutions quantified using an attractive interparticle force. *Langmuir* **35**, 10533–10541 (2019).
21. M. R. W. Scheepers, S. R. R. Haenen, J. M. Coers, L. J. van IJzendoorn, M. W. J. Prins, Inter-particle biomolecular reactivity tuned by surface crowders. *Nanoscale* **12**, 14605–14614 (2020).
22. J. G. Wetmur, Hybridization and renaturation kinetics of nucleic acids. *Annu. Rev. Biophys. Bioeng.* **5**, 337–361 (1976).
23. J. G. Wetmur, N. Davidson, Kinetics of renaturation of DNA. *J. Mol. Biol.* **31**, 349–370 (1968).
24. L. P. Reynaldo, A. V. Vologodskii, B. P. Neri, V. I. Lyamichev, The kinetics of oligonucleotide replacements. *J. Mol. Biol.* **297**, 511–520 (2000).
25. N. Sugimoto, S. Nakano, M. Yoneyama, K. Honda, Improved thermodynamic parameters and helix initiation factor to predict stability of DNA duplexes. *Nucleic Acids Res.* **24**, 4501–4505 (1996).
26. K. J. Breslauer, R. Frank, H. Blöcker, L. A. Marky, Predicting DNA duplex stability from the base sequence. *Proc. Natl. Acad. Sci. U.S.A.* **83**, 3746–3750 (1986).
27. T. Strunz, K. Oroszlan, R. Schäfer, H. J. Güntherodt, Dynamic force spectroscopy of single DNA molecules. *Proc. Natl. Acad. Sci. U.S.A.* **96**, 11277–11282 (1999).
28. R. W. L. van Vliembergen, L. J. van IJzendoorn, M. W. J. Prins, Nanoscale interparticle distance within dimers in solution measured by light scattering. *Langmuir* **34**, 179–186 (2018).
29. P. Varilly, S. Angioletti-Uberti, B. M. Mognetti, D. Frenkel, A general theory of DNA-mediated and other valence-limited colloidal interactions. *J. Chem. Phys.* **137**, 094108 (2012).